Monthly Notices
of the
ROYAL ASTRONOMICAL SOCIETY

Mon. Not. R. Astron. Soc. **422,** 3081–3091 (2012) doi:10.1111/j.1365-2966.2012.20879.x

# The effects of baryon physics, black holes and active galactic nucleus feedback on the mass distribution in clusters of galaxies

Davide Martizzi,[1]★ Romain Teyssier,[1,2] Ben Moore[1] and Tina Wentz[1]

[1]*Institute for Theoretical Physics, University of Zurich, CH-8057 Zürich, Switzerland*
[2]*CEA Saclay, DSM/IRFU/SAP, Bâtiment 709, F-91191 Gif-sur-Yvette, Cedex, France*

Accepted 2012 February 24. Received 2012 February 21; in original form 2011 December 12

**ABSTRACT**

The spatial distribution of matter in clusters of galaxies is mainly determined by the dominant dark matter component; however, physical processes involving baryonic matter are able to modify it significantly. We analyse a set of 500 pc resolution cosmological simulations of a cluster of galaxies with mass comparable to Virgo, performed with the AMR code RAMSES. We compare the mass density profiles of the dark, stellar and gaseous matter components of the cluster that result from different assumptions for the subgrid baryonic physics and galaxy formation processes. First, the prediction of a gravity-only $N$-body simulation is compared to that of a hydrodynamical simulation with standard galaxy formation recipes, and then all results are compared to a hydrodynamical simulation which includes thermal active galactic nucleus (AGN) feedback from supermassive black holes (SMBHs). We find the usual effects of overcooling and adiabatic contraction in the run with standard galaxy formation physics, but very different results are found when implementing SMBHs and AGN feedback. Star formation is strongly quenched, producing lower stellar densities throughout the cluster, and much less cold gas is available for star formation at low redshifts. At redshift $z = 0$ we find a flat density core of radius 10 kpc in both the dark and stellar matter density profiles. We speculate on the possible formation mechanisms able to produce such cores and we conclude that they can be produced through the coupling of different processes: (I) dynamical friction from the decay of black hole orbits during galaxy mergers; (II) AGN-driven gas outflows producing fluctuations of the gravitational potential causing the removal of collisionless matter from the central region of the cluster; (III) adiabatic expansion in response to the slow expulsion of gas from the central region of the cluster during the quiescent mode of AGN activity.

**Key words:** black hole physics – methods: numerical – galaxies: clusters: general – galaxies: formation – cosmology: theory – large-scale structure of Universe.

## 1 INTRODUCTION

Clusters of galaxies are the most massive virialized structures observed in the Universe and provide a wonderful laboratory to test astrophysical theories. In the Λ cold dark matter (ΛCDM) cosmological scenario, clusters are assembled via a hierarchy of mergers of less massive structures like galaxies and groups of galaxies. Many physical processes play a role during the formation of a cluster. When satellite galaxies are accreted into a cluster, their properties can be changed by tidal and ram pressure stripping, leading to the formation of a wide variety of galaxy morphologies. Furthermore, clusters are known to be dark matter dominated structures, with most of the baryonic matter residing in a hot diffuse X-ray emitting gaseous phase, the intracluster medium. The stellar mass is less significant and mainly contained in the massive central elliptical galaxy.

Since they are dominated by dark matter, this mass component determines the global properties of the mass distribution in the cluster. However, from the theoretical side, it is well known that baryonic processes can produce significant differences in the distribution of matter in collapsed structures with respect to models including only collisionless CDM. For example, baryons are known to condense the centre of dark matter haloes due to dissipative processes, producing adiabatic contraction of the total mass distribution (Gnedin et al. 2004). Several models including baryonic physics have been invoked to solve the so-called cusp/core problem in the ΛCDM cosmological framework, i.e. the discrepancy between the centrally cuspy dark matter profiles observed in dark matter haloes in numerical $N$-body simulations and the centrally cored dark matter profiles

★E-mail: martdav@physik.uzh.ch

inferred by observations in dwarf galaxies and low surface brightness galaxies (see the recent review by de Blok 2010, and references therein). The study of baryon physics induced modifications in the mass distribution in collapsed structures, and clusters of galaxies in particular, is still a field with many open issues.

This paper is dedicated to the study of the effects of baryonic processes on the mass distribution in clusters of galaxies. In particular, we use a set of cosmological hydrodynamical simulations performed using the AMR code RAMSES (Teyssier 2002) to study the effect of different models for baryons and galaxy formation physics on the mass density profile of a cluster of galaxies comparable to the Virgo cluster. This work can be considered as an extension of the analysis performed by Teyssier et al. (2011) on the same simulations, and is complementary to the analysis presented by Martizzi, Teyssier & Moore (2012). Here, we focus on the peculiar properties produced in the mass density profile when including supermassive black holes (SMBHs) and the related AGN feedback in the recipes for galaxy formation physics. We stress that AGN feedback was initially introduced to solve the so-called 'overcooling problem', namely the fact that too much stellar mass is produced in massive collapsed structure in hydrodynamical simulations with respect to what is observed in the real Universe (Borgani & Kravtsov 2009). The strong quenching of star formation produced by processes that couple AGN activity with the gas is expected to improve the match between simulations and observations (Tabor & Binney 1993; Ciotti & Ostriker 1997; Silk & Rees 1998). Strong evidence for the existence of AGN feedback is provided by observations of X-ray cavities and radio blobs in galaxy clusters, typically interpreted as buoyantly rising bubbles of high-entropy material injected in the central region of clusters by jets of relativistic particles. In this paper, we show that by including SMBH physics and AGN feedback it is possible to obtain interesting predictions on the modifications they can induce on the mass distribution in massive dark matter haloes.

The paper is organized as follows: the first section is dedicated to the numerical methods and the galaxy formation recipes adopted for our simulations; we show our main results and provide our interpretation in the second section; the last section is left for a short summary of our results and a discussion.

## 2 NUMERICAL METHODS

In this section, we describe the numerical techniques used to model the cluster we consider in this paper. We consider two cosmological hydrodynamical simulations presented in Teyssier et al. (2011) and Martizzi et al. (2012), plus a third cosmological simulation with only dark matter. For all the three runs we used the AMR code RAMSES (Teyssier 2002). The simulations were performed using the zoom-in technique which allows us to obtain the required effective resolution only in selected regions of the computational domain. For all the three simulations the computational domain is a cubic box of side 100 Mpc $h^{-1}$. For the dark matter only run (DMO, Tables 1 and 2) run we adopt a standard ΛCDM cosmology with parameters $\Omega_{\rm m} = 0.3$, $\Omega_\Lambda = 0.7$, $\Omega_{\rm b} = 0.0$, $\sigma_8 = 0.77$ and $H_0 = 70\ {\rm km\,s^{-1}\,Mpc^{-1}}$. For the two hydrodynamical runs (HYDRO runs in Tables 1 and 2) we adopt the same values for $\Omega_{\rm m}$, $\Omega_\Lambda$, $\sigma_8$ and $H_0$, but we set $\Omega_{\rm b} = 0.045$. The initial conditions for the three simulations were computed using the Eisenstein & Hu (1998) transfer function and the GRAFIC package (Bertschinger 2001) in its parallel implementation MPGRAFIC (Prunet et al. 2008). To perform the zoom-in technique we adopted the following approach: first, we ran a low-resolution DMO simulation, and then we identified dark matter haloes at $z = 0$. From this halo catalogue we built a set of haloes whose virial masses lie in the range $10^{14}$ to $2 \times 10^{14}\,{\rm M_\odot}\,h^{-1}$. Finally, we identified the final halo based on its assembly history: the halo is already in place at $z = 1$; therefore, it can be considered as relaxed at $z = 0$. In particular the last major merger is observed at redshift $z \sim 1.3$. The final virial mass is $M_{\rm vir} \simeq 10^{14}\,{\rm M_\odot}$, while $M_{\rm 200c} = 1.04 \times 10^{14}\,{\rm M_\odot}$ or $M_{\rm 500c} = 7.80 \times 10^{13}\,{\rm M_\odot}$, where index $c$ refers to the critical density. This halo has been resimulated at higher resolution, focusing the computational resources in the region of the computational domain where it forms.

**Table 1.** Cosmological parameters adopted in our simulations. The DMO label refers to the dark matter only run. The HYDRO label refers to the hydrodynamical runs.

| Type | $H_0$ (km s$^{-1}$ Mpc$^{-1}$) | $\sigma_8$ | $\Omega_\Lambda$ | $\Omega_{\rm m}$ | $\Omega_{\rm b}$ |
|---|---|---|---|---|---|
| | Cosmological parameters | | | | |
| DMO | 70 | 0.77 | 0.7 | 0.3 | – |
| HYDRO | 70 | 0.77 | 0.7 | 0.3 | 0.045 |

**Table 2.** Mass resolution for dark matter particles, gas cells and star particles and spatial resolution (in physical units) for our two sets of simulations.

| Type | $m_{\rm cdm}$ ($10^6\,{\rm M_\odot}\,h^{-1}$) | $m_{\rm gas}$ ($10^6\,{\rm M_\odot}\,h^{-1}$) | $m_*$ ($10^6\,{\rm M_\odot}\,h^{-1}$) | $\Delta x_{\rm min}$ (kpc $h^{-1}$) |
|---|---|---|---|---|
| | Mass and spatial resolution | | | |
| DMO | 9.6 | n.a. | n.a. | 0.38 |
| HYDRO | 8.2 | 1.4 | 0.3 | 0.38 |

In the DMO simulations the dark matter particle in the high-resolution region has a mass of $9.6 \times 10^6\,{\rm M_\odot}\,h^{-1}$. In the two hydrodynamical runs, the dark matter particle in the high-resolution region has a mass of $8.2 \times 10^6\,{\rm M_\odot}\,h^{-1}$, whereas the baryon resolution element has a mass of $1.4 \times 10^6\,{\rm M_\odot}\,h^{-1}$. Hydrodynamics is solved on an AMR grid that was initially refined to the same level of refinement as the particle grid ($2048^3$, level $\ell = 11$). During the runs, seven more levels of refinement were considered (level $\ell_{\rm max} = 18$). The refinement criterion we used allows spatial resolution to be roughly constant in physical units; the minimum cell physical size was always close to $\Delta x_{\rm min} = L/2^{\ell_{\rm max}} \simeq 500\,{\rm pc}\,h^{-1}$. The grid was dynamically refined using a quasi-Lagrangian strategy: when the dark matter or baryons mass in a cell reaches eight times the initial mass resolution, it is split into eight children cells.

In the HYDRO runs, gas dynamics is modelled using a second-order unsplit Godunov scheme (Teyssier 2002; Fromang, Hennebelle & Teyssier 2006; Teyssier, Fromang & Dormy 2006) based on the HLLC Riemann solver and the MinMod slope limiter (Toro, Spruce & Speares 1994). We assume a perfect gas equation of state with $\gamma = 5/3$. The HYDRO runs include standard subgrid models for gas cooling (accounting for H, He and metals; we use the Sutherland & Dopita 1993 cooling function), star formation (we adopt a star formation efficiency $\epsilon_* = 0.01$) and supernovae feedback (we adopt the 'delayed cooling' scheme; Stinson et al. 2006) and metal enrichment. In one of the two hydrodynamical simulations we also implement AGN feedback, using a modified version of the Booth & Schaye (2009) model. SMBHs are modelled as sink particles, following the prescriptions of Krumholz, McKee & Klein (2004), and they are allowed to merge. Gas accretion on to each SMBH is computed adopting a modified Bondi–Hoyle formula (Booth & Schaye 2009). A fraction of the accreted mass is

converted into thermal energy that is directly injected into the gas surrounding the black hole (BH). For practical purposes, in the rest of the paper we will refer to the run with AGN feedback as AGN-ON, and to the run without AGN feedback as AGN-OFF. Further details about the galaxy formation and AGN feedback recipes can be found in Martizzi et al. (2012) and Teyssier et al. (2011).

As discussed in Teyssier et al. (2011), the AGN feedback energy is effectively deposited in two different modes: the energetic and impulsive quasar mode (Eddington limited luminosity $\sim 5 \times 10^{46}\,\mathrm{erg\,s^{-1}}$) during cold gas accretion when the accretion rate is high, and the quiescent radio mode during hot gas accretion when the accretion rate is low (Bondi–Hoyle limited luminosity $\sim 5 \times 10^{41}\,\mathrm{erg\,s^{-1}}$). At $z \sim 0$ the central SMBH in the AGN-ON cluster accretes mass in radio mode at a rate $\sim 10^{-4}\,\mathrm{M_\odot\,yr^{-1}}$, producing a total luminosity of $9 \times 10^{40}\,\mathrm{erg\,s^{-1}}$, comparable to the X-ray luminosity of the AGN in M87 $L_{\mathrm{X},0.5-7\,\mathrm{keV}} \approx 7 \times 10^{40}\,\mathrm{erg\,s^{-1}}$ (Allen et al. 2006); the mechanical power of the jet of the AGN in M87 is much larger, $P \approx 3.3 \times 10^{43}\,\mathrm{erg\,s^{-1}}$. These considerations imply that the AGN in M87 lies in an intermediate state between the radio and the quasar modes of our model. Further indications that the activity of the central SMBH is not particularly atypical are provided by comparison of the accretion rates and star formation rates in the AGN-ON simulation with observational results at redshift $z \sim 0$. The mass accretion rate on to the SMBH is $\sim 10^{-4}\,\mathrm{M_\odot\,yr^{-1}}$ and the star formation rate within the inner few kpc from the cluster centre is $\sim 10^{-2}\,\mathrm{M_\odot\,yr^{-1}}$. These values are comparable with those recently measured by Diamond-Stanic & Rieke (2012) for type 1 Seyfert galaxies.

## 3 RESULTS

In this section, we show how SMBHs and AGN feedback are able to change dramatically the properties of the mass distribution in clusters of galaxies. We focus on 3D mass density profiles of the cluster, analysing separately the dark matter and stellar components, as well as the total mass distribution. The goal is to highlight differences between the profiles in the DMO, AGN-ON and AGN-OFF runs. The interpretation of our main results is provided in the next section.

### 3.1 Mass density profiles at redshift $z = 0$

Spherically averaged mass density profiles of the cluster at redshift $z = 0$ have been computed for all the simulations. A reliable identification of halo centres is required to compute density profiles. Halo centres and virial radii have been identified using the AdaptaHOP algorithm (Aubert, Pichon & Colombi 2004), in the version implemented and tested by Tweed et al. (2009), using the most massive substructure method (MSM) to identify haloes as well as their substructures. AdaptaHOP can be used to find the centres of groups of dark matter particles (i.e. 'haloes') as well as groups of star particles in the HYDRO runs (i.e. 'galaxies'). In the DMO run we directly use the centre of the dark matter halo, whereas in the AGN-ON and AGN-OFF runs we use the centre of the most massive group of star particles (i.e. the centre of the brightest cluster galaxy) since it traces better the minimum of the gravitational potential. To test that the latter choice does not lead to errors in the estimate of the profiles in the inner region of the cluster, we verified that picking the halo centre instead of the galaxy centre does not change the measured profiles.

Fig. 1 shows the dark matter and stellar mass density profiles at $z = 0$ for the AGN-ON (solid line) and AGN-OFF (dashed line) runs; in this plot we use physical units. In the left-hand panel the result of the DMO run (dotted line) is also plotted for comparison. All the profiles extend to the virial radius of the cluster. The three dark matter profiles look quite similar in the outer regions ($r \gtrsim 50\,\mathrm{kpc}$), while they are significantly different in the inner regions. The AGN-OFF profile is much more centrally peaked and concentrated than the DMO profile, a result that can be interpreted as a result of adiabatic contraction of dark matter haloes in response to the condensation of baryons at their centres (Gnedin et al. 2004; Teyssier et al. 2011); we test the quality of adiabatic contraction models in reproducing our results in Subsection 3.2. The AGN-ON profile is much different, with a very shallow inner slope. Within the inner 10 kpc we observe a dark matter core whose size is much larger than our spatial resolution limit (grey shaded area), whereas the AGN-OFF and DMO profiles seem to be consistent with cuspy dark matter profiles. Observational support to the results of our AGN-ON model comes from studies where gravitational lensing and dynamical data are combined to estimate the dark matter

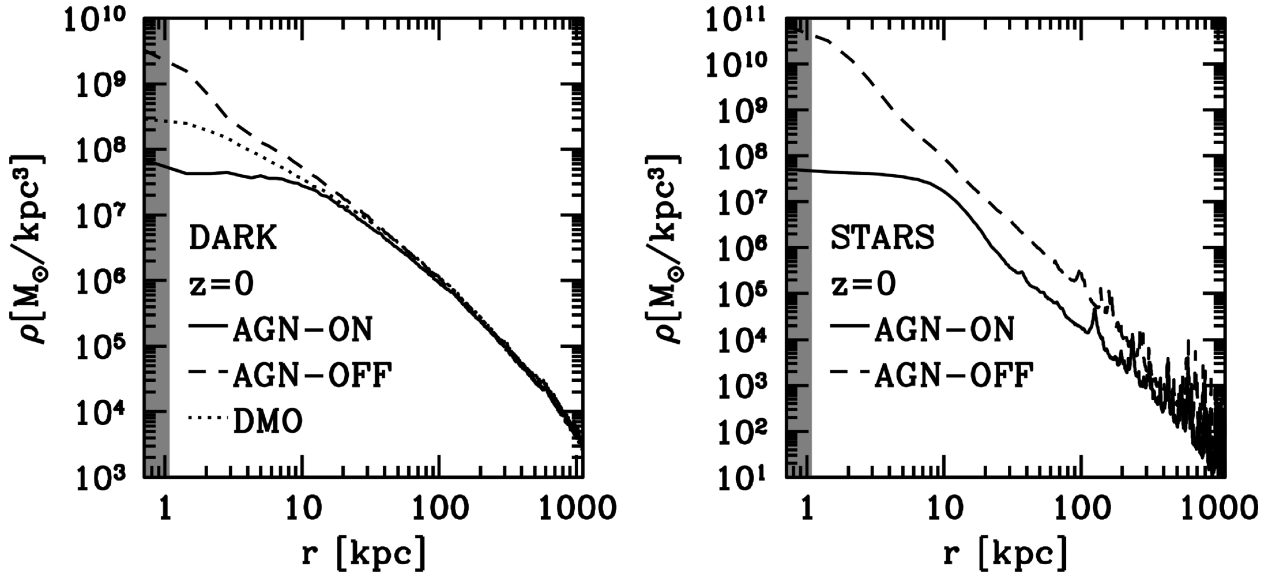


**Figure 1.** Mass density profiles at $z = 0$. Left: dark matter. Right: stars. In all panels the grey shaded area represents the spatial resolution.

profiles of clusters of galaxies (Sand et al. 2004, 2008; Newman et al. 2009, 2011; Richtler et al. 2011): these studies provide significative evidence of the existence of clusters of galaxies with dark matter profiles presenting cores or shallower inner slopes than in the Navarro–Frenk–White model.

Looking at the stellar mass density profiles, we see that significantly less stellar mass forms in the AGN-ON run with respect to the AGN-OFF run that is affected by overcooling. At $r > 50$ kpc the stellar mass density in the AGN-OFF run is $\sim$10 times bigger than in the AGN-ON run in all the radial bins, and a very significative difference can be observed between the two profiles within $\sim$10 kpc from the centre: the AGN-OFF density profile is increasing towards the centre, whereas the AGN-ON profile shows a flat core with a size comparable to that observed in the dark matter profile. It is interesting that cores in the stellar surface brightness profiles of very massive elliptical galaxies and cluster central galaxies have been observed by several authors (Kormendy 1999; Quillen, Bower & Stritzinger 2000; Laine et al. 2003; Trujillo et al. 2004; Lauer et al. 2005; Côté et al. 2007; Kormendy et al. 2009; Graham 2011) and they can be deprojected in cored 3D stellar density profiles (Terzić & Graham 2005).

In the AGN-OFF cluster the mass budget in the central region is strongly dominated by stellar mass: in the absence of AGN feedback the star formation process is very efficient in turning gas into stars; the large stellar mass in the central region of the AGN-OFF cluster has been assembled through cooling flows providing gaseous material to trigger intense star formation events and through the accretion of satellite galaxies on to the central galaxy. In contrast, the mass in the central regions of the AGN-ON cluster has comparable contributions from stars and dark matter: overcooling is prevented from happening by AGN feedback and star formation is strongly quenched.

### 3.2 Dark matter profiles at $z = 0$: testing the adiabatic contraction model

It is possible to estimate some of the effects of baryonic processes, SMBHs and AGN feedback using an approach similar to that used by observers when analysing the surface brightness profiles of galaxies. First, an analytical model is used to fit the profile, and then any significant deviation from the model is interpreted as a signature of physical processes. The same approach has been used to detect central light excesses/deficiencies with respect to a Sérsic fit to the surface brightness profiles of early-type galaxies (Kormendy et al. 2009; Graham 2011). In Martizzi et al. (2012) we also adopted this approach to discuss the properties of the stellar core observed in the stellar mass density profile in the AGN-ON run, showing that the Sérsic function can be used to fit the stellar mass surface density profile outside the cored region. Here, we use this criterion to analyse the dark matter profiles we measure in our simulations at $z = 0$.

We adopt the Einasto profile as our fiducial analytical model, since it has been shown to provide excellent fits to the dark matter profiles observed in cosmological $N$-body simulations (Merritt et al. 2005; Graham et al. 2006). We use the following parametrization:

$$\rho_{\rm Ein}(r) = \rho_{\rm e} \exp\left\{-d_n \left(\frac{r}{r_{\rm e}}\right)^{1/n} - 1\right\}, \quad (1)$$

where

$$d_n = 3n - 1/3 - 0.0079/n. \quad (2)$$

We use this analytical function to fit the dark matter profiles at $z = 0$, leaving $I_{\rm e}$, $n$ and $r_{\rm e}$ as free parameters. Our fits are performed using the Levenberg–Marquardt non-linear least-squares fit algorithm (Press et al. 1992). The parameters we obtain after the fits are summarized in Table 3. In the DMO case we measure a concentration $c_{200} = R_{200c}/R_{-2} = 5.88$, where $R_{-2}$ is the radius at which the logarithmic slope of the dark matter profile is $-2$. This value is typical for haloes of mass $\sim 10^{14}\,{\rm M}_\odot$ (Reed, Koushiappas & Gao 2011).

The fits are compared to the measured profiles in Fig. 2. The Einasto profile provides a very good fit to the dark matter profile of our halo in the DMO run, despite the fact that it is typically used to fit the average profile in cosmological simulations whereas we analyse only one halo. Both in the AGN-ON and AGN-OFF we observe that the Einasto profile is a good fit for $r > 10$ kpc, while we observe significative deviations with respect to the fitting formula in the inner regions (see the bottom-right panel of Fig. 2). The presence of these features can be interpreted as a manifestation of processes that influence the formation of a standard distribution of dark matter in phase space; since these features are not observed in the gravity-only DMO run, we try to give them an explanation in terms of baryon physics.

Dark matter haloes are expected to respond adiabatically to the condensation of baryons at their centres (Gnedin et al. 2004; Teyssier et al. 2011). We compare the results of our hydrodynamical runs at $z = 0$ with the prediction of a simple adiabatic contraction model used by Abadi et al. (2010), and already adopted in Teyssier et al. (2011); details of this model can be found in Appendix A. We adiabatically contract the Einasto fit to the DMO profile assuming that the baryons are distributed in a constant surface density, truncated sphere of mass $m_{\rm d}$ and radius $r_{\rm d}$, despite the fact that the actual distribution is different. The values of $m_{\rm d}$ and $r_{\rm d}$ adopted in this paper are shown in Table 4. The result is plotted in Fig. 2 (blue lines): in both the AGN-ON and AGN-OFF cases the adiabatically contracted profiles match the Einasto fits quite well at all radii, but, like the fits, the model does not provide a satisfactory description of the measured profiles for $r < 10$ kpc. A mass excess with respect to the adiabatic contracted profile is detected in the AGN-OFF case.

**Table 3.** Best-fitting parameters $\rho_{\rm e}$, $r_{\rm e}$ and $n$ for the Einasto profile at redshift $z = 0$. The value of the reduced chi-squared $\widetilde{\chi}^2$ (1386 d.o.f.) for $10 < r < 1000$ kpc is also reported. The values are reported for the DMO, AGN-ON and AGN-OFF simulations.

| Simulation | $\rho_{\rm e}({\rm M}_\odot\,{\rm kpc}^{-3})$ | $r_{\rm e}$(kpc) | $n$ | $\widetilde{\chi}^2$ |
|---|---|---|---|---|
| | | Einasto profile fits – $z = 0$ | | |
| DMO | $1.43 \times 10^3 \pm 1.5 \times 10^2$ | $1.60 \times 10^3 \pm 6 \times 10^1$ | $5.93 \pm 1.2 \times 10^{-1}$ | 0.94 |
| AGN-ON | $1.39 \times 10^3 \pm 1.1 \times 10^2$ | $1.55 \times 10^3 \pm 5 \times 10^1$ | $5.65 \pm 9 \times 10^{-2}$ | 0.97 |
| AGN-OFF | $6.2 \times 10^2 \pm 9 \times 10^1$ | $2.0 \times 10^3 \pm 1.1 \times 10^2$ | $7.38 \pm 1.8 \times 10^{-1}$ | 2.21 |

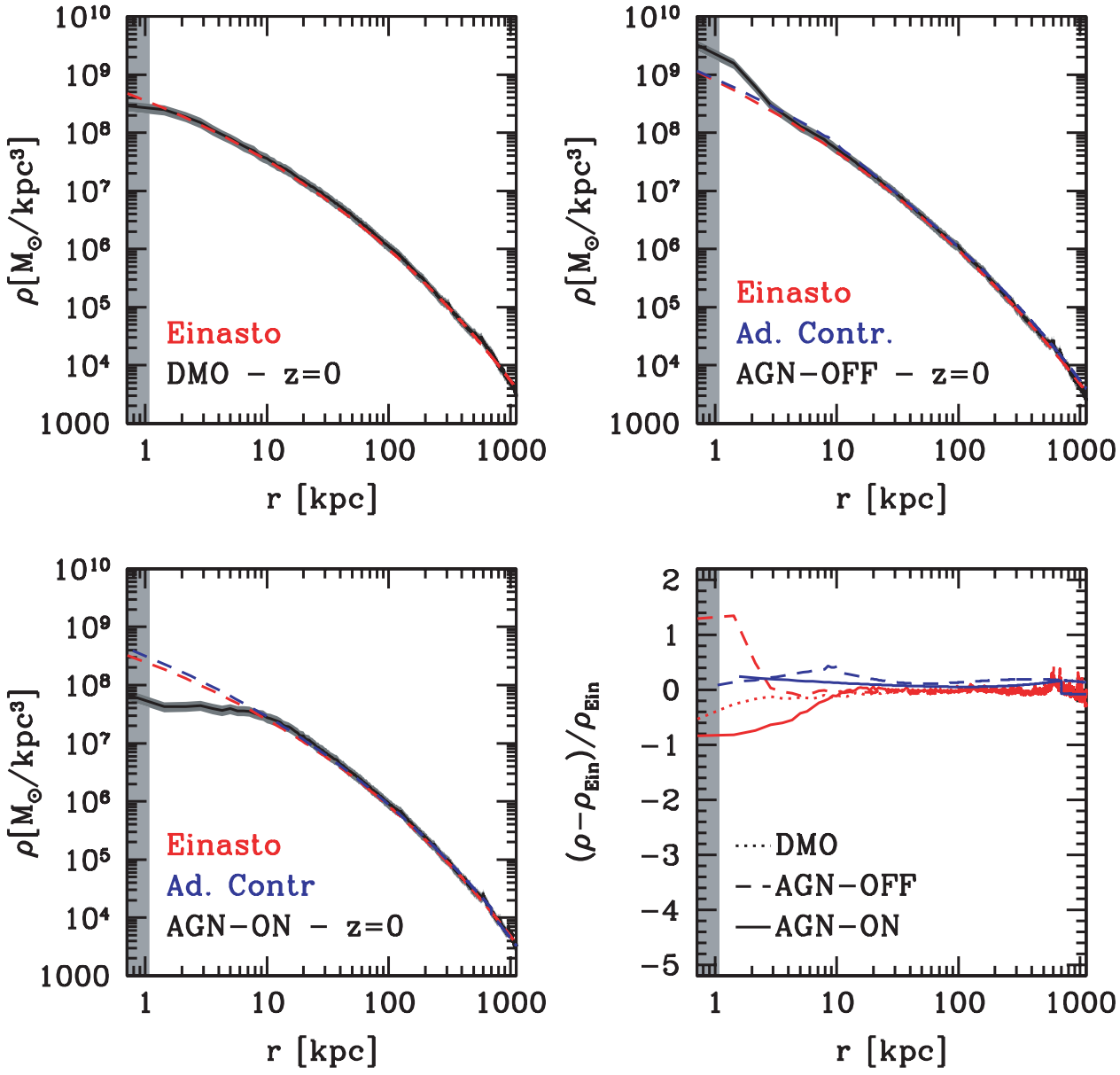


**Figure 2.** Comparison between the dark matter profiles measured at redshift $z = 0$ (black solid lines) and the Einasto fits (red dashed lines). The scatter due to Poisson noise in each radial bin is also represented as a dark-grey shaded area. The DMO Einasto fit is adiabatically contracted to get the two blue dashed profiles. Top-left panel: DMO run. Top-right panel: AGN-OFF run. Bottom-left panel: AGN-ON run. Bottom-right panel: relative difference between the measured profile and the Einasto fit as a function of radius (red lines); we use a dotted line for the DMO run, a dashed line for the AGN-OFF run and a solid line for the AGN-ON run; the blue lines show the residuals of the adiabatic contraction models with respect to the Einasto fits. In all panels the grey shaded area represents the spatial resolution.

**Table 4.** Parameters adopted for the adiabatic contraction model: truncated sphere mass $m_{\rm d}$ and radius $r_{\rm d}$.

| Simulation | $m_{\rm d}$ ($\rm M_\odot$) | $r_{\rm d}$ (kpc) |
|---|---|---|
| Adiabatic contraction model parameters | | |
| AGN-ON | $1.7 \times 10^{13}$ | 700 |
| AGN-OFF | $2.6 \times 10^{11}$ | 10 |

The adiabatic contraction model works reasonably well, especially at radii beyond a few kpc. In the interval $10 < r < 1000$ kpc we measure reduced chi-squared values for the adiabatic contraction models $\widetilde{\chi}^2 = 2.14$ for the AGN-OFF case and $\widetilde{\chi}^2 = 0.72$ for the AGN-ON case. These values are quite similar to what we obtain for the Einasto fits in the same radial range (Table 3).

In the AGN-ON run we find a mass deficiency with respect to the adiabatically contracted profile within 10 kpc from the centre; this mass deficiency is $M_{\rm def} = 5.7 \times 10^{10}\,\rm M_\odot$. The fact that adiabatic contraction works for the outer regions of the cluster, but cannot predict the formation of the core, highlights the fact that additional processes play a role in shaping the properties of the mass distribution. Given the theoretical and computational limits of our phenomenological model for AGN feedback and the formation of SMBHs, and given that we limit our analysis to the evolution of one halo, these results provide evidence that SMBH physics is indeed relevant in shaping the properties of clusters of galaxies,

especially in the most overdense regions where SMBHs are expected to be found. We will discuss these topics in further detail in Subsection 3.4.

### 3.3 Evolution of the mass density profiles

The study of the evolution of the mass density profiles in our simulations can be used to shed more light on the mechanisms through which SMBHs and AGN feedback influence the mass distribution in clusters. To do so, we found the centres of the most massive progenitors of the cluster in each simulation, computed density profiles at redshifts $z = 1, 2, 3, 4, 5$ and then compared to the result at $z = 0$. All the profiles shown in this subsection are plotted in physical units.

First of all, we analyse the dark matter profile evolution in the DMO simulation (Fig. 3). In the outskirts of the cluster, the profiles change their slope; this transition marks the virial radius of the cluster. At redshift $z = 5$ the mass distribution in the halo is still quite different than at later times, with a shallower central slope and a radius $R_{200c} \approx 60$ kpc. At later times the inner part of the profiles ($r \lesssim 20$ kpc) reaches stability and evolution can be observed only in the outskirts where additional mass collapses into the halo; in fact, the high $r$ tail of the profile is constantly extending towards bigger distances from the centre. At redshift $z = 0$ we measure that $R_{200c} \approx 1$ Mpc. This kind of evolution is a clear example of stable clustering.

In Fig. 4 we show the evolution of the dark and stellar mass density profiles in the AGN-OFF run. The effect of adiabatic contraction due to the condensation of baryonic mass at the centre of the cluster is already evident at redshift $z = 5$: the density within the inner 10 kpc is almost an order of magnitude larger than in the DMO case. Similarly to the DMO case, as the dark matter halo is assembled, the dark matter profile in the inner region appears to be stable from $z = 4$ to 0, while additional dark mass appears to be accreted at higher radii. The stellar mass profiles evolve maintaining its shape, but increasing in amplitude. New stars are constantly formed and a significant increase of the stellar mass can be observed between all the considered snapshots.

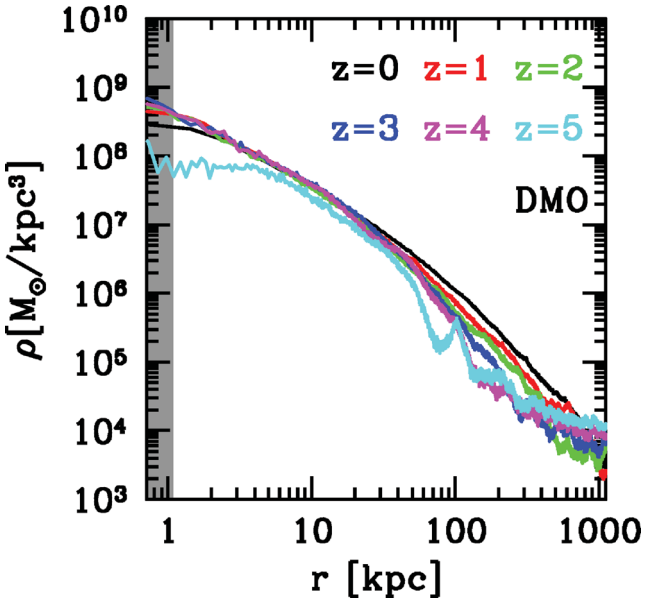


**Figure 3.** Evolution of the dark matter density profile in the DMO run from $z = 5$ to 0. The grey shaded area represents the spatial resolution.

Finally, Fig. 5 shows the same profiles for the AGN-ON run, highlighting some of the most interesting peculiarities of our model. The evolution of the dark matter profile in the outer regions of the cluster ($r \gtrsim 20$ kpc) is very similar to that observed in the DMO case, but the inner region is strikingly different. The effects of the processes leading to the formation of the core observed at $z = 0$ can be directly observed. At redshift $z = 5$ the dark matter profile appears to be contracted with respect to the DMO case, but much less than in the AGN-OFF case. Instead of maintaining the original slope, like in the AGN-OFF case, the inner part of the dark matter profiles becomes shallower with time, until a core is formed. A very similar behaviour is observed for the stellar mass density profile. While stellar mass is always increasing with time at radii $r \gtrsim 20$, the inner profile evolves in a very peculiar way: at redshift $z = 5$ the stellar profile is very cuspy, but it evolves becoming shallower and shallower, despite the fact that the total stellar mass within 10 kpc from the centre increases. Between $z = 1$ and 0 the stellar profile becomes almost completely flat for $r < 10$ kpc.

### 3.4 Formation of central cores in the density profile

The most evident peculiarity of the mass distribution in our AGN-ON simulation is the central core observed in the stellar and dark matter density profiles. From the plots (Fig. 5) in the previous subsection we see that the dark matter core forms more gradually than the stellar core. At $z > 1$ we see that the dark matter profile gradually evolves towards a cored configuration, while the stellar profile builds up maintaining its cuspy inner shape. The most interesting transition towards the formation of the two cores happens between redshifts $z = 1$ and 0: in this interval the dark matter profile becomes extremely flat, while the cusp at the centre of the stellar profile is completely erased. The fact that this behaviour is not observed in the AGN-OFF simulation suggests that the cores in the AGN-ON dark and stellar matter profiles do not form naturally, but they are generated through external processes influencing the dynamics of collisionless matter. The aim of this subsection is to elucidate the mechanisms that lead to core formation in our simulated cluster.

Several models have been proposed to produce cores in the density profile of a distribution of collisionless matter starting from a cuspy profile; these models were originally developed to explain the dark matter cores observed in gas-rich dwarf galaxies (de Blok 2010), but may be applied, in principle, to any distribution of collisionless matter. El-Zant, Shlosman & Hoffman (2001) showed that sufficiently massive gas clumps can disrupt cusps through dynamical friction; this is not observed in our AGN-ON run since gas clouds are easily disrupted by AGN feedback. El-Zant et al. (2004) showed that galaxies moving within the dark matter background and transferring their orbital energy to the dark matter via dynamical friction may contribute to the formation of cores. More recently, the very high resolution simulation of Naab, Johansson & Ostriker (2009) showed a similar effect: repeated minor dry mergers lead to decreases of the central stellar density concentration. This result has been confirmed by subsequent numerical experiments, like those presented by Laporte et al. (2012). The dense cores of accreted galaxies able to survive for a few crossing times modify the stellar mass distribution through dynamical friction. We emphasize that the same principle applies to the dark matter component, due to its collisionless nature. This effect is not observed in our AGN-OFF run because completely dry mergers are rare due to the high gas fractions in galaxies in this simulation. In the AGN-ON run, instead, a significant fraction of the gas is expelled from galaxies and the Naab et al. (2009) mechanism can be more efficient.

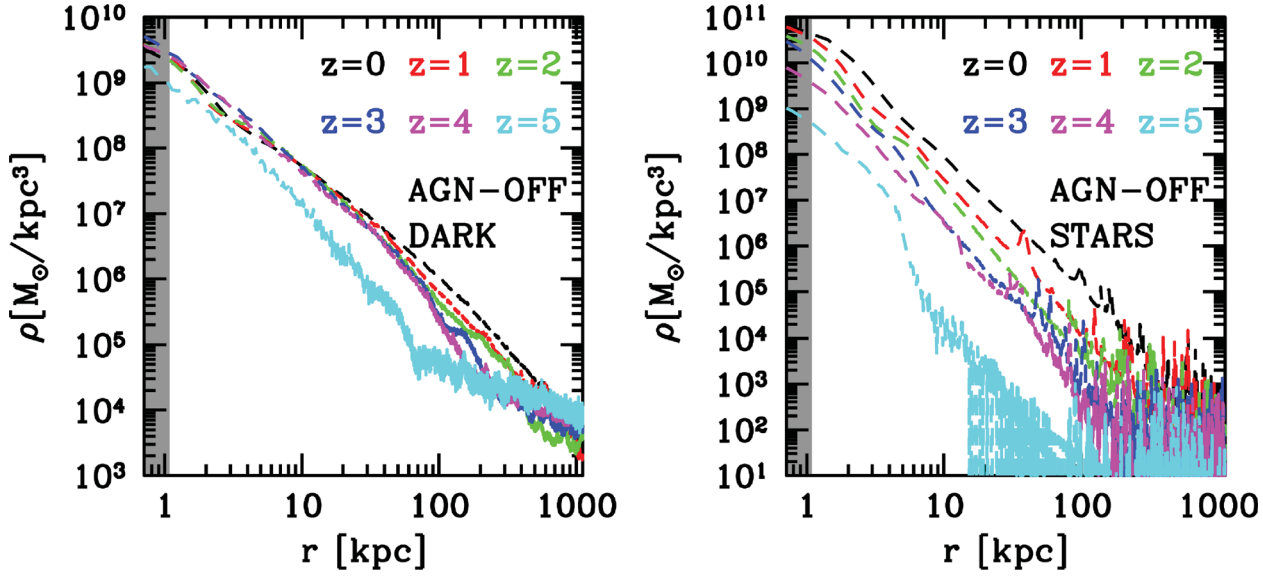


**Figure 4.** Evolution of the density profiles in the AGN-OFF run from $z = 5$ to 0. Left: dark matter. Right: stars. In all panels the grey shaded area represents the spatial resolution.

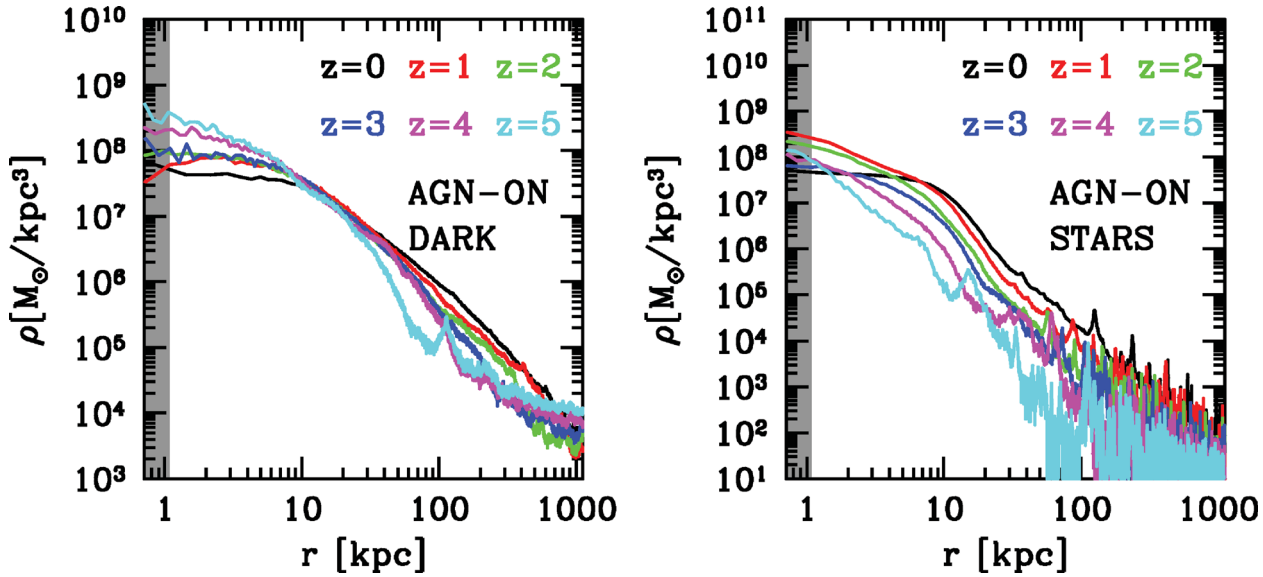


**Figure 5.** Evolution of the density profiles in the AGN-ON run from $z = 5$ to 0. Left: dark matter. Right: stars. In all panels the grey shaded area represents the spatial resolution.

Unfortunately, it seems to be challenging to produce an extended flat core like the one observed in our AGN-ON model only through repeated dry minor mergers.

Alternative mechanisms to produce cores in dark matter profiles involve purely gravitational processes related to SMBHs. In the context of a ΛCDM cosmology, where massive structures form through the hierarchical mergers of less massive structures, the formation of SMBH binaries is an expected result. At the centre of collapsed objects SMBHs form binary pairs whose orbits decay as they transfer their orbital energy to collisionless matter via three-body interactions: the result is that collisionless matter can be expelled from the central regions via the gravitational slingshot effect and a core is formed. This process is usually referred to as SMBH scouring (Milosavljević & Merritt 2003) and it is expected to remove approximately two to four times the mass of the SMBH formed after the binary completely decays (Merritt, Mikkola & Szell 2007). SMBH scouring is important on spatial scales from 100 to 1 pc; thus, it cannot be resolved in our simulations which has 1 kpc force softening. At the softening length the mass is completely dominated by dark matter and stars so that SMBH binaries cannot form.

Despite the fact that SMBH scouring is not resolved in our simulations, they are able to resolve another process able to produce cores, namely SMBHs sinking to the very central region due to dynamical friction during mergers. The efficiency of this process has been extensively studied by Goerdt et al. (2010) and their results show that the orbital energy transferred from the SMBHs to collisionless matter contributes to the formation of cores. The efficiency of this process is not as high as in the SMBH scouring, but

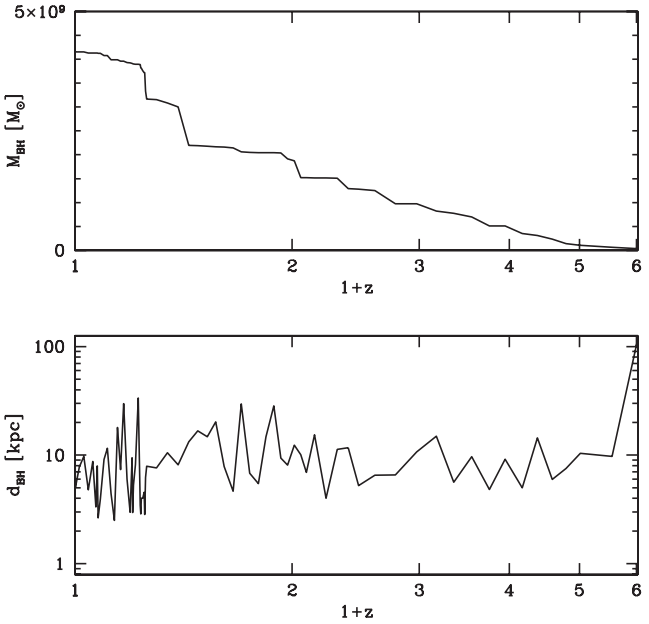


**Figure 6.** Top: evolution of the central SMBH observed at redshift $z = 0$. Bottom: evolution of the distance between the central SMBH observed at redshift $z = 0$ and its closest neighbour.

it is able to produce mass deficiencies comparable to the mass of the infalling SMBHs. In our AGN-ON simulation the mass of the central SMBH at $z = 0$ is $M_{\rm BH} = 4.2 \times 10^9\,{\rm M}_\odot$, so this process by itself is not able to explain the mass deficiencies we observe in the central regions of the cluster: $M_{\rm def}^{\rm dark} = 5.7 \times 10^{10}\,{\rm M}_\odot$ for dark matter and $M_{\rm def}^{\rm star} = 3.04 \times 10^{10}\,{\rm M}_\odot$ for stars, measured with respect to an Einasto fit and a Sérsic fit to the entire profile, respectively.

Recently, the pure $N$-body simulations performed by Kulkarni & Loeb (2012) showed that when multiple (two or more) SMBHs are present in a halo, the core formation process is much more efficient than during the inspiral of a single SMBH. Considering this enhanced core formation via dynamical friction it is possible to create mass deficits of more than five times the total SMBH mass. The top panel of Fig. 6 shows the mass growth of the central SMBH at the centre of the cluster at $z = 0$. The mass growth of this BH is very smooth for $z > 2$, but it proceeds mainly through major mergers (sudden jumps in the BH mass) at lower redshifts. The bottom panel of Fig. 6 shows the distance between the central SMBH and its closest neighbour as a function of redshift, denoted as $d_{\rm BH}$. Any sudden increase in the SMBH mass $M_{\rm BH}$ due to a BH merger in the top-panel plot can be detected as an increase in $d_{\rm BH}$, because after mergers the second neighbour becomes the first neighbour. The continuous variation of $d_{\rm BH}$ tells us that at any redshift BHs are moving in the halo and losing orbital energy because of dynamical friction. A significative number of major mergers of very massive BHs happen at $z < 1$. This fact suggests that the Kulkarni & Loeb (2012) mechanism is particularly efficient at redshifts $z < 1$.

SMBH infall is not the only process contributing to the formation of the core. In the AGN-ON simulation strong AGN-driven outflows are observed (Martizzi et al. 2012). AGN feedback greatly increases the local temperature and entropy of gas; then the high-entropy material is transported out of the central region of the cluster through convective motions. These outflows modify the local gravitational potential and may cause expansion of both the dark and stellar mass distribution. Similar processes have been observed in numerical simulations in which gas outflows generated by supernovae feedback are used to produce cores in the dark matter profiles of dwarf galaxies (Navarro, Eke & Frenk 1996; Gnedin & Zhao 2002; Read & Gilmore 2005; Governato et al. 2010; Pontzen & Governato 2011). In the simulations performed by Navarro et al. (1996), the mass outflows are simulated by growing and rapidly removing an idealized potential from the centre of an equilibrium realization of a dark matter halo, showing that the natural consequence is the formation of a core. The efficiency of this core formation process is $\propto M_{\rm disc}^{1/2} R_{\rm disc}^{-1/2}$, where $M_{\rm disc}$ is the mass of the disc and $R_{\rm disc}$ is its scale radius.

The calculations performed by Gnedin & Zhao (2002) show that this mechanism is extremely inefficient when a single supernova explosion is considered; however, Read & Gilmore (2005) showed that repeated explosions followed by gas outflows and subsequent infalls are able to account for the formation of dark matter cores. The recent numerical experiments performed by Governato et al. (2010) and Pontzen & Governato (2011) confirm the efficiency of this mechanism in a fully cosmological context. In particular, Pontzen & Governato (2011) suggest that gravitational potential fluctuations induced by supernovae-driven outflows happening on a time-scale shorter than the dynamical time cause the expansion of the dark matter distribution and the formation of a core. For this mechanism to be effective it is required to have gas outflows able to remove a significant fraction of the mass enclosed in the region where the core forms. Since we have multiple epochs of AGN-driven gas outflows, this mechanism is likely to be active also in our AGN-ON run. This is indeed the case: Fig. 7 shows that the gas mass fluctuations induced by AGN burst-driven outflows can be high fractions of the total mass in the central regions. Regions close to the central SMBH (radius $r < R = 2$–$5$ kpc) present extreme mass fluctuations on short time-scales. Within $r < R = 10$ kpc fluctuations become smaller, but can be as large as 10 per cent of the enclosed total mass. At higher distances from the centre the effect of these mass fluctuations is almost undetected. This means that potential fluctuations will be particularly strong only within the inner 10 kpc from the centre, that is the region where the core is observed. It is interesting to note that the amplitude of the mass fluctuations is

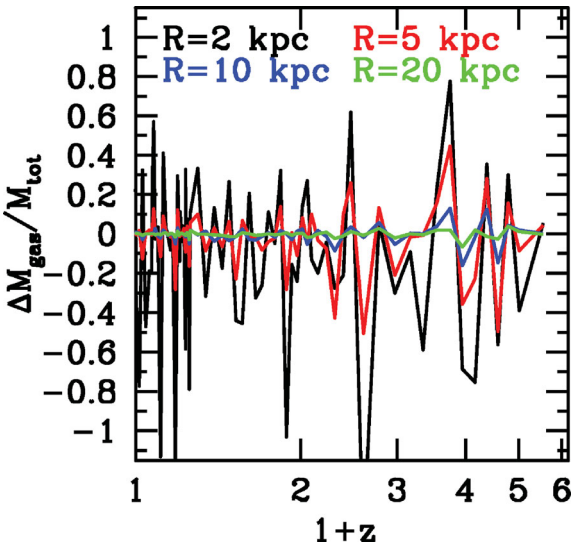


**Figure 7.** Variation of the gas mass enclosed in spheres of radius $R = 2$, 5, 10 and 20 physical kpc with respect to the total mass in the same region. The absolute value of the fluctuations can be larger than 1 because the variation of the gas mass is divided by the total mass after the outflow.

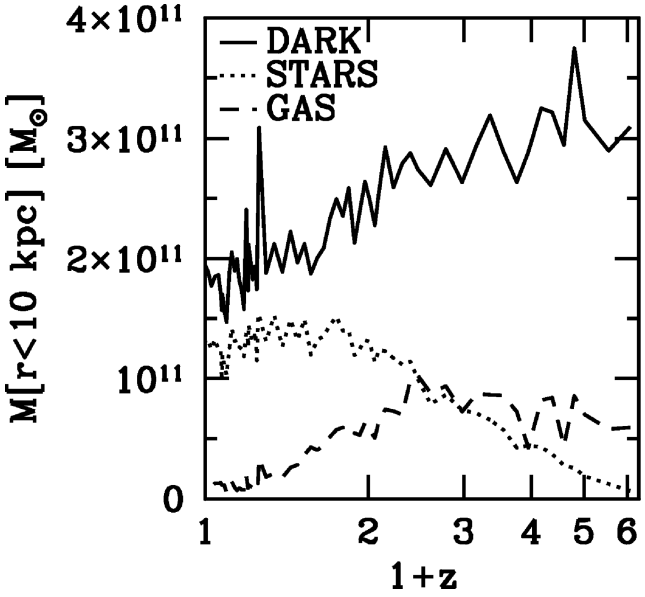


**Figure 8.** Time evolution of the total dark, stellar and gas mass enclosed within 10 physical kpc in the AGN-ON run.

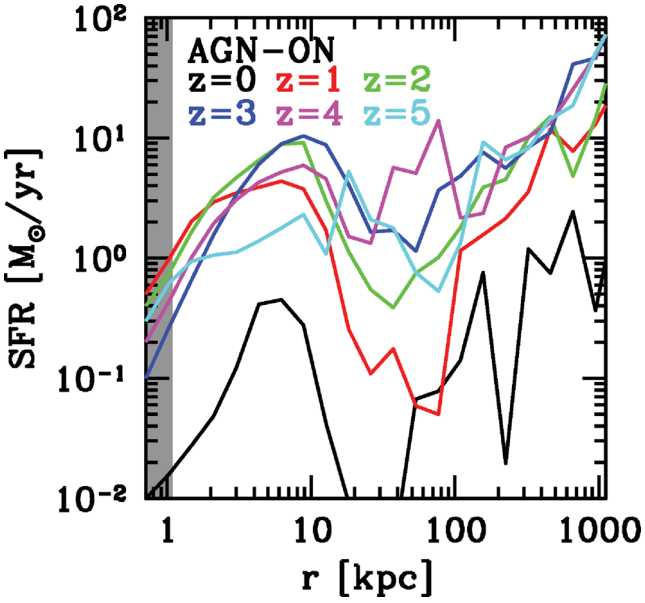


**Figure 9.** Average star formation rate in radial bins in the AGN-ON run. The grey shaded area represents the spatial resolution.

typically higher at $z > 1$; however, quite strong fluctuations are also observed at low redshift.

Before drawing our conclusions, we carefully analyse what happens in the central region of the cluster. Fig. 8 shows how the mass distribution in the central region of the cluster is influenced by the core formation mechanisms. We plot the evolution of the mass enclosed within 10 physical kpc for all the different components: dark matter (solid lines), stars (dotted lines) and gas (dashed lines). The core formation processes produce a decrease in the dark mass within 10 kpc from the centre from $\sim 3 \times 10^{11}\,\mathrm{M}_{\odot}$ at $z = 5$ to $\sim 2 \times 10^{11}\,\mathrm{M}_{\odot}$ at $z = 0$. The stellar mass in the centre increases with time only down to $z = 1$, staying approximately constant until $z = 0$. At high redshift the star formation rate in the central region is high and the concentration of the stellar mass distribution is boosted by star formation events (Fig. 9); at redshift $z < 1$ the star formation in the central galaxy is strongly quenched by AGN feedback (Fig. 9), so the concentration of the stellar distribution cannot be boosted by strong star formation events, thus letting the core formation processes be effective. At $z < 1$ when AGN feedback becomes very strong because of the presence of very massive BHs, a slow decrease in the gas mass in the centre is observed: a gas mass $\sim 10^{11}\,\mathrm{M}_{\odot}$ is slowly removed from the central region before $z = 0$. This slow decrease in gas mass is expected to produce an adiabatic expansion of the total mass distribution, which will also contribute to the formation of a central core. Furthermore, the cooling time of hot gas within the inner 30 kpc of the cluster centre is $\sim 1$ Gyr, suggesting that in its quiet mode the AGN can slowly eject the gas that rains down on to the centre from the inner cooling flow.

The general picture we find from our analysis seems to show that the interplay between dynamical processes connected to SMBHs and the effects of AGN feedback on the star formation and the gas spatial distribution may provide an explanation to what is observed in our simulations. The dark matter core starts forming at redshift $z = 4$–$5$ due to AGN burst-driven gas mass fluctuations on short time-scales. The process goes on with very high efficiency down to redshift $z = 1$. At redshift $z < 1$ the infall of very massive SMBHs contributing to the core formation process compensates for the smaller amplitude of the gas mass fluctuations. The final result is a flat dark matter core at redshift $z = 0$. The formation of the stellar core proceeds quite differently, with star formation compensating for the ejection of stellar material at $z > 1$, preventing the early formation of a core. At $z < 1$ the decrease in the star formation rate caused by AGN feedback finally allows the stellar core to form by redshift $z = 0$.

Given our conclusions, we must stress that a clearer picture on the core formation problem has still to be drawn. The problem needs to be studied within a larger class of haloes with different merger histories and masses, and idealized simulations are probably required to shed more light on the core formation process in clusters.

## 4 SUMMARY AND CONCLUSIONS

We used the results of a set of cosmological simulations to study the effect of baryons in massive dark matter haloes, focusing on phenomena involving SMBHs and AGN feedback. We use the zoom-in technique to simulate the formation of a galaxy cluster of mass comparable to Virgo at high spatial and mass resolution. In this work we analyse three different simulations: the first is a gravity-only run with no baryons (DMO), the second is a hydrodynamical run with standard galaxy formation physics (AGN-OFF), the third is a hydrodynamical run with standard galaxy formation physics plus SMBHs and AGN feedback (AGN-ON). We adopt a modified version of the Booth & Schaye (2009) model to implement thermal AGN feedback in the AGN-ON run. This model allows us to reproduce the self-regulated growth of BHs throughout the cosmic ages and it is tuned to reproduce the observed $M_{\mathrm{BH}}$–$\sigma$ relation.

Our analysis focuses on the evolution of the 3D mass density profiles of the cluster from redshift $z = 5$ to 0. We find a number of interesting differences between our models that highlight the importance of accounting for all the physical processes taking place during the formation and evolution of the most massive bound structures in the Universe. Our results can be summarized in the following points.

(i) At redshift $z = 0$ the dark matter density profiles of the three simulations are consistent with each other at distances $r > 10$ kpc from the centre, but they differ significantly in the central region. The DMO profile is consistent with a standard Einasto model. The AGN-OFF profile shows a mass excess with respect to an Einasto fit due to adiabatic contraction of the baryons at the centre of the cluster. The AGN-ON profile presents a flat core of radius 10 kpc, i.e. a mass deficiency with respect to an Einasto fit. The dark matter core forms gradually from $z = 5$ to 0. We stress that dark matter cores in dark matter profiles have been claimed to be observed in several clusters (Sand et al. 2004, 2008; Newman et al. 2009, 2011; Richtler et al. 2011).

(ii) The stellar density profile at $z = 0$ is also very different between the AGN-OFF and AGN-ON runs. The AGN-OFF profile is very peaked at the centre, while the AGN-ON profile has a core of the same size as that of the dark one. Unlike the dark core, the stellar one forms between $z = 1$ and 0. Note that cores in the surface brightness profiles of massive ellipticals and cluster central galaxies have been observed by several authors (Kormendy 1999; Quillen et al. 2000; Laine et al. 2003; Trujillo et al. 2004; Lauer et al. 2005; Côté et al. 2007; Kormendy et al. 2009; Graham 2011), so our model is not in disagreement with observations and it *predicts* the existence of dark matter cores associated with stellar cores in massive ellipticals. Furthermore, in the AGN-OFF run the stellar density is larger than that in the AGN-ON run at all radii. This is a clear effect of overcooling of gas leading to enhanced (and too efficient) star formation. In the AGN-ON run, AGN feedback strongly quenches star formation and the overcooling problem is avoided (Martizzi et al. 2012; Teyssier et al. 2011). The result is also that less cool gas is available at the centre of the AGN-ON cluster with respect to the AGN-OFF run: gas is heated by AGN feedback and carried away via convective motions and slow adiabatic expansion.

(iii) The core in the dark matter and stellar mass density profiles is a peculiar feature of our simulation that includes the physics associated with AGNs. In this paper, we suggest that the coupling of several mechanisms is responsible for their formation. First, SMBHs transfer part of their orbital energy to collisionless matter via dynamical friction during dry galaxy mergers (Goerdt et al. 2010), especially at redshift $z < 1$. Secondly, AGN-driven gas outflows modify the gravitational potential in regions close to SMBHs with resulting ejection of collisionless matter from the central region of the cluster; subsequent gas outflows followed by the central 're-virialization' of the central material are expected to produce cores (Pontzen & Governato 2011); due to the stronger AGN feedback at $z > 1$, this mechanism is more effective at high redshift, but preserves an important role at low redshift. Thirdly, the central hot gas slowly cools radiatively, falling on to the SMBHs in convective flows and is subsequently ejected impulsively; the slow loss of mass from the central region will produce an expansion of the inner mass distribution.

Despite assertions that AGN feedback can affect central cluster dynamics, in fact our results seem to be complementary to the those obtained by other authors for less massive dark matter haloes (Governato et al. 2010; Maccio' et al. 2012; Pontzen & Governato 2011). Related processes involving baryons seem to be active at the low and high mass end of the galaxy mass function, especially mechanisms involving gas outflows produced by feedback.

Given the fact that we perform the analysis on zoom simulations of one cluster, we need to stress that our result needs support from a suite of dedicated cosmological simulation aimed at exploring the effect of SMBHs, AGN feedback and baryon physics in general on the most massive clusters in the universe. Furthermore, a number of numerical experiments are also needed to explore in detail the core formation processes that have been considered in our discussion, with particular attention on their coupling. The role of baryon mass outflows in galaxy clusters has been recently studied by Ragone-Figueroa, Granato & Abadi (2012) using collisionless matter simulations where gas is modelled as a time varying external contribution to the gravitational potential; their results provide important support to ours. To conclude, we are convinced that our results are robust enough to assert that the implementation of AGN feedback and SMBHs in cosmological hydrodynamical simulations is an important ingredient for modelling massive clusters of galaxies.

## ACKNOWLEDGMENT

The AMR simulations presented here were performed on the Cray XT-5 cluster at CSCS, Manno, Switzerland.

## REFERENCES

Abadi M. G., Navarro J. F., Fardal M., Babul A., Steinmetz M., 2010, MNRAS, 407, 435
Allen S. W., Dunn R. J. H., Fabian A. C., Taylor G. B., Reynolds C. S., 2006, MNRAS, 372, 21
Aubert D., Pichon C., Colombi S., 2004, MNRAS, 352, 376
Bertschinger E., 2001, ApJS, 137, 1
Booth C. M., Schaye J., 2009, MNRAS, 398, 53
Borgani S., Kravtsov A., 2009, preprint (arXiv:0906.4307)
Ciotti L., Ostriker J. P., 1997, ApJ, 487, L105
Côté P. et al., 2007, ApJ, 671, 1456
de Blok W. J. G., 2010, Adv. Astron., 789293
Diamond-Stanic A. M., Rieke G. H., 2012, ApJ, 746, 168
Eisenstein D. J., Hu W., 1998, ApJ, 496, 605
El-Zant A., Shlosman I., Hoffman Y., 2001, ApJ, 560, 636
El-Zant A. A., Hoffman Y., Primack J., Combes F., Shlosman I., 2004, ApJ, 607, L75
Fromang S., Hennebelle P., Teyssier R., 2006, A&A, 457, 371
Gnedin O. Y., Zhao H., 2002, MNRAS, 333, 299
Gnedin O. Y., Kravtsov A. V., Klypin A. A., Nagai D., 2004, ApJ, 616, 16
Goerdt T., Moore B., Read J. I., Stadel J., 2010, ApJ, 725, 1707
Governato F. et al., 2010, Nat, 463, 203
Governato F. et al., 2010, Nat, 463, 203
Graham A. W., 2011, preprint (arXiv:1108.0997)
Graham A. W., Merritt D., Moore B., Diemand J., Terzić B., 2006, AJ, 132, 2701
Kormendy J., 1999, in Merritt D. R., Valluri M., Sellwood J. A., eds, ASP Conf. Ser. Vol. 182, The Central Structure of Elliptical Galaxies and the Stellar-Dynamical Search for Supermassive Black Holes. Astron. Soc. Pac., San Francisco, p. 124
Kormendy J., Fisher D. B., Cornell M. E., Bender R., 2009, ApJS, 182, 216
Krumholz M. R., McKee C. F., Klein R. I., 2004, ApJ, 611, 399
Kulkarni G., Loeb A., 2012, MNRAS, doi:10.1111/j.1365-2966.2012.20699.x
Laine S., van der Marel R. P., Lauer T. R., Postman M., O'Dea C. P., Owen F. N., 2003, AJ, 125, 478
Laporte C. F. P., White S. D. M., Naab T., Ruszkowski M., Springel V., 2012, preprint (arXiv:1202.2357)
Lauer T. R. et al., 2005, AJ, 129, 2138
Maccio' A. V., Stinson G., Brook C. B., Wadsley J., Couchman H. M. P., Shen S., Gibson B. K., Quinn T., 2012, ApJ, 744, L9
Martizzi D., Teyssier R., Moore B., 2012, MNRAS, 420, 2859
Merritt D., Navarro J. F., Ludlow A., Jenkins A., 2005, ApJ, 624, L85
Merritt D., Mikkola S., Szell A., 2007, ApJ, 671, 53
Milosavljević M., Merritt D., 2003, ApJ, 596, 860

Naab T., Johansson P. H., Ostriker J. P., 2009, ApJ, 699, L178
Navarro J. F., Eke V. R., Frenk C. S., 1996, MNRAS, 283, L72
Newman A. B., Treu T., Ellis R. S., Sand D. J., Richard J., Marshall P. J., Capak P., Miyazaki S., 2009, ApJ, 706, 1078
Newman A. B., Treu T., Ellis R. S., Sand D. J., 2011, ApJ, 728, L39
Pontzen A., Governato F., 2012, MNRAS, doi:10.1111/j.1365-2966.2012.20571.x
Press W. H., Teukolsky S. A., Vetterling W. T., Flannery B. P., 1992, Numerical Recipes in C. The Art of Scientific Computing. Cambridge Univ. Press, Cambridge
Prunet S., Pichon C., Aubert D., Pogosyan D., Teyssier R., Gottloeber S., 2008, ApJS, 178, 179
Quillen A. C., Bower G. A., Stritzinger M., 2000, ApJS, 128, 85
Ragone-Figueroa C., Granato G. L., Abadi M. G., 2012, preprint (arXiv:1202.1527)
Read J. I., Gilmore G., 2005, MNRAS, 356, 107
Reed D. S., Koushiappas S. M., Gao L., 2011, MNRAS, 415, 3177
Richtler T., Salinas R., Misgeld I., Hilker M., Hau G. K. T., Romanowsky A. J., Schuberth Y., Spolaor M., 2011, A&A, 531, A119
Sand D. J., Treu T., Smith G. P., Ellis R. S., 2004, ApJ, 604, 88
Sand D. J., Treu T., Ellis R. S., Smith G. P., Kneib J.-P., 2008, ApJ, 674, 711
Silk J., Rees M. J., 1998, A&A, 331, L1
Stinson G., Seth A., Katz N., Wadsley J., Governato F., Quinn T., 2006, MNRAS, 373, 1074
Sutherland R. S., Dopita M. A., 1993, ApJS, 88, 253
Tabor G., Binney J., 1993, MNRAS, 263, 323
Terzić B., Graham A. W., 2005, MNRAS, 362, 197
Teyssier R., 2002, A&A, 385, 337
Teyssier R., Fromang S., Dormy E., 2006, J. Comput. Phys., 218, 44
Teyssier R., Moore B., Martizzi D., Dubois Y., Mayer L., 2011, MNRAS, 414, 195
Toro E. F., Spruce M., Speares W., 1994, Shock Waves, 4, 25
Trujillo I., Erwin P., Asensio Ramos A., Graham A. W., 2004, AJ, 127, 1917
Tweed D., Devriendt J., Blaizot J., Colombi S., Slyz A., 2009, A&A, 506, 647

## APPENDIX A: ADIABATIC CONTRACTION MODEL

The simplified model we adopt is based on that used in Teyssier et al. (2011). If one defines the initial radius of each dark matter shell as $r_\mathrm{i}$, then an adiabatic contraction model is able to predict its value after contraction $r_\mathrm{f}$. In our case we adopt the transformation

$$\frac{r_\mathrm{f}}{r_\mathrm{i}} = 1 + \alpha \left( \frac{M_\mathrm{i}}{M_\mathrm{f}} - 1 \right), \tag{A1}$$

where $M_\mathrm{i}$ and $M_\mathrm{f}$ are the cumulative mass distributions before and after contraction, respectively. The final cumulative mass distribution can be computed as

$$M_\mathrm{f} = M_\mathrm{dm}(r_\mathrm{f}) + M_\mathrm{bar}(r_\mathrm{f}) = f_\mathrm{dm} M_\mathrm{i}(r_\mathrm{i}) + M_\mathrm{bar}(r_\mathrm{f}), \tag{A2}$$

where $M_\mathrm{i}(r_\mathrm{i})$ is the initial mass distribution in the DMO case, $M_\mathrm{bar}(r_\mathrm{f})$ is the baryonic mass distribution and $M_\mathrm{dm}(r_\mathrm{f})$ is the adiabatically contracted dark matter distribution. The dark mass fraction is computed as $f_\mathrm{dm} = 1 - m_\mathrm{d}/M_{200}$. Our aim is to recover the contracted dark matter profile $M_\mathrm{dm}(r_\mathrm{f})$ given $M_\mathrm{i}(r_\mathrm{i})$ and $M_\mathrm{bar}(r_\mathrm{f})$. We assume that the $M_\mathrm{i}(r_\mathrm{i})$ can be described by the fit to the Einasto profile we obtain for the DMO run at redshift $z = 0$:

$$M_\mathrm{i}(r_\mathrm{i}) = 4\pi \int_0^{r_\mathrm{i}} r^2 \rho_\mathrm{Ein}(r)\, \mathrm{d}r. \tag{A3}$$

The baryonic mass distribution is modelled as a constant surface density sphere with size $r_\mathrm{d}$ and mass $m_\mathrm{d}$:

$$M_\mathrm{bar}(r_\mathrm{f}) = \begin{cases} m_\mathrm{d} \left( \frac{r_\mathrm{f}}{r_\mathrm{d}} \right)^2 & \text{if } r < r_\mathrm{d} \\ m_\mathrm{d} & \text{if } r \geq r_\mathrm{d}. \end{cases}$$

We obtain the $r_\mathrm{f}$ value associated with each $r_\mathrm{i}$ solving numerically equation (A1), and naturally obtain the adiabatically contracted dark matter profile $M_\mathrm{dm}(r_\mathrm{f})$ using equation (A2). Finally, we estimate the dark matter density profile after contraction as

$$\rho_\mathrm{dm}(r) = \frac{1}{4\pi r^2} \frac{\mathrm{d}M_\mathrm{dm}(r)}{\mathrm{d}r}. \tag{A4}$$

This paper has been typeset from a TEX/LATEX file prepared by the author.